

# Role of the North Atlantic in Indian Monsoon Droughts

P. J. Borah<sup>1</sup>, V. Venugopal<sup>1,2,\*</sup>, J. Sukhatme<sup>1</sup>, P. Muddebihal<sup>1</sup> and B. N. Goswami<sup>3</sup>

<sup>1</sup>Centre for Atmospheric and Oceanic Sciences &  
Divecha Centre for Climate Change  
Indian Institute of Science, Bangalore 560012, India.

<sup>2</sup> Interdisciplinary Centre for Water Research  
Indian Institute of Science, Bangalore, 560012, India.

<sup>3</sup> Department of Physics, Cotton University, Guwahati 781001, India.

\*Correspondence: E-mail: [venu.vuruputur@gmail.com](mailto:venu.vuruputur@gmail.com) –or– [venu@iisc.ac.in](mailto:venu@iisc.ac.in)

## Abstract

The forecast of Indian monsoon droughts has been predicated on the notion of a season-long rainfall deficit linked to warm anomalies in the equatorial Pacific. Here, we show that in fact nearly half of all droughts over the past century were sub-seasonal, and characterized by an abrupt decline in late-season rainfall. Furthermore, the potential driver of this class of droughts is a coherent cold anomaly in the North Atlantic Ocean. The vorticity forcing associated with this oceanic marker extends through the depth of the troposphere, and results in a wavetrain which curves towards the equator and extends to East-Asia. This upper-level response triggers an anomalous low-level anticyclonic circulation late in the season over India. This teleconnection from the midlatitudes offers an avenue for improved predictability of monsoon droughts.

Embedded within the interannual and intraseasonal variability of Indian summer monsoon rainfall (ISMR) [1, 2, 3, 4, 5] are complex space-time patterns pertaining to its extreme states, namely, floods and droughts [4, 6, 7]. Given that the socio-economic fabric of one sixth of the world's population is intricately tied to the state of the monsoon [8], these extremes, especially droughts, have a devastating impact on agriculture and the economy. Against this backdrop, despite its high potential predictability [9], the forecast of ISMR one season in advance remains a grand challenge [10, 11, 12]. For instance, it is known that anomalously warm waters in the equatorial central/eastern Pacific (El Niño) are associated with some ISMR droughts [13, 14, 15, 16]. However, the dynamics, or what drives droughts not associated with El Niño has remained mostly unknown. Added to this is the prevailing notion that ISMR droughts are characterized by large-scale season-long rainfall deficit. Indeed, a deeper insight into droughts via their sub-seasonal evolution is essential not only for a better understanding of these extremes, but also practically for targeted improvement of general circulation models in realizing the potential for improved ISMR prediction.

Over the past century, India has experienced 23 droughts and, as identified in [Table S1](#), 13 of these occurred with, and 10 that occurred without, an El Niño [17]. These two flavors of droughts are henceforth referred to as EN + Dr and NEN + Dr, respectively. This sea surface temperature (SST) based classification is confirmed in Figs. 1a and 1b, which show the mean of detrended SST anomalies during June through September (JJAS) for the years listed in [Table S1](#). Both types of droughts (Fig. 1c), though significantly different from normal years, are statistically indistinguishable from each other at 5% significance level ( $p$ -value = 0.09) on a seasonal scale ([Fig. S1](#)). Given the disparate oceanic conditions associated with the two kinds of droughts, we investigate their sub-seasonal evolution to similar final seasonal states.

Figure 2a shows the temporal behavior of daily anomalies of area-averaged central India rainfall (16.5N-26.5N; 74.5E-86.5E; see methods) during JJAS, for the two categories, in comparison to normal years. The daily anomalies for each of the drought years are shown in [Fig. S2](#), from which the averages shown in Fig. 2a are estimated. The difference in the evolution of the two droughts is immediately evident. Specifically, in the EN + Dr category (thin red curve in Fig. 2a), negative rainfall anomalies, i.e., departures from the daily climatological mean, set in during mid-

June and persist till early August. On the other hand, in NEN + Dr (thin blue curve in Fig. 2a), anomalies have more rapid and intense fluctuations culminating in an abrupt drop (also, long break; mid-to-late-August period highlighted by the blue ellipse in Fig. S2b) during mid-August. The envelopes (thick curves) of these two flavors of droughts, represented by their respective leading harmonics ( $\sim 120, 60, 40$  days), reinforces this distinction. The genesis of these “climatological sub-seasonal oscillations” [18] is plausibly linked to a preferred temporal clustering of “breaks” across the years in the respective categories (red and blue ellipses in Fig. S2).

The stark difference in timing and duration of the breaks in these two categories is captured in Fig. 2b, which shows the respective composites of the cumulative of daily rainfall anomalies (see Fig. S3 for individual years). A comparison of these cumulatives also shows that NEN + Dr has a larger overall deficit than EN + Dr till early July and recovers around mid-July. While the timing may be different, the rate of change (drop) in both categories is about 2-2.5 mm/d (0 to -100 mm in  $\sim 45$  days during June-July for EN + Dr vs -25 mm to -75 mm in 20 days during mid-to-late August for NEN + Dr). The final state of the two curves in Fig. 2b is in accord with the fact that, on average, the magnitude of the seasonal deficit is larger in EN + Dr (17%) than in NEN + Dr (13%), as can be inferred from Table S1. While the discussion so far has revolved around central India, the distinction between the two categories of droughts holds for all of India as well (Fig. S4). Thus, an examination of the daily rainfall evolution of all droughts in the past century reveals that EN and NEN droughts are seasonal and sub-seasonal phenomena, respectively.

Returning to the original basis of our classification, namely, SSTs, while EN + Dr has a well-defined warm anomaly extending into the central Pacific (Fig. 1a), the only prominent feature that stands out in the second category (NEN + Dr) is a strong and coherent negative SST anomaly in the North Atlantic ocean (Fig. 1b). The association of El Niño with monsoon droughts, characterized by a season-long rainfall deficit, has been extensively explored [15, 19, 20]. Here, we focus on the latter category (NEN + Dr), hitherto less explored [17], and provide a mechanistic explanation of how conditions over the North Atlantic lead to an abrupt late season decline in rainfall over India, resulting in a sub-seasonal drought.

The seasonal (JJAS) wind anomaly, averaged for NEN + Dr years, over this North Atlantic oceanic marker, is shown in Fig. 3. The equivalent barotropic nature of the regional atmospheric

response is evident and consists of a cyclonic circulation that extends all the way from 850 mb, where it is compact, to 200 mb, where it expands, intensifies and becomes more zonal in character. The teleconnection from the North Atlantic to the Indian region is examined by analyzing upper tropospheric winds during the long break in Indian monsoon rainfall (days 81-90; see Fig. 2b). Specifically, Figs. 4a and 4b show the interaction of the upper level flow with this persistent and deep tropospheric vorticity forcing (Fig. 3) during this period. The resultant 200 mb meridional wind anomalies (shading in Fig. 4a) indicate a response to the east of the Atlantic that has a large footprint extending all the way to East Asia [21, 22]. At 500 mb (Fig. 4b), as expected, the anomalies are weaker; more interestingly, the response curves towards the equator, with a prominent signature over the Indian region, apparently guided by the Tibetan plateau (the narrowing of the wind anomalies to the east of 60°E in Fig. 4b). The anticyclonic nature of wind anomalies over North India, signs of which are evident at 500 mb, becomes clearer at lower levels (700 mb and 850 mb; Fig. 4c and 4d). This circulation anomaly not only weakens the zonal flow over the Arabian Sea (i.e., disrupting the Somali Jet), but also strengthens and spreads to cover all of India, as we descend from 700 mb to 850 mb. Contrasting this with the low-level cyclonic circulation over India, 20 days prior to the break (Fig. S5), highlights the abruptness of this phenomenon.

Our results establish that NEN droughts are sub-seasonal and are a consequence of remote columnar atmospheric forcing above a persistent cold North Atlantic SST anomaly. From a broader perspective, the association of the Atlantic basin with Indian summer monsoon has been explored, albeit mostly on decadal and interannual timescales [23, 24, 25, 26, 27, 28, 29]. It is worth noting that nearly all NEN droughts occur during the negative phase of the Atlantic Multidecadal Oscillation (AMO; see Fig. S6). Even though all “cold” North Atlantic episodes do not necessarily result in a monsoon drought, they cause a break during the monsoon following the mechanism elucidated above (see Figs. S7, S8 and “Supplementary Text”).

While the teleconnection (wave train) from the North Atlantic vorticity forcing to the Indian region appears to be robust, the role of SST in the development of this forcing needs further investigation. In recent years, there is increased recognition that SST anomalies can trigger a deep tropospheric response in the midlatitudes [30, 31, 32]. To better understand this in our context, we examine the total columnar vorticity in years with negative and positive SST anomalies in the

North Atlantic (Fig. S9a). It is quite evident from Fig. S9b that there is a propensity for a cyclonic (anti-cyclonic) environment over the North Atlantic in years when the SST anomaly is negative (positive). Equally importantly, even though the SST anomaly stays negative through JJAS, the columnar vorticity anomalies are episodic, with a tendency to occur in June and August, and persist for 2 to 3 weeks (Fig. S9b). As would be expected, vorticity anomalies during NEN + Dr years, which have on an average colder anomaly, show a similar build up (blue curve in Fig. S9b), but are amplified significantly (see Supplementary Text and Table S3) in August [33]. Thus, while SST anomalies may not be solely responsible, they seem to be essential in the formation of a transient deep tropospheric circulation in this region.

Taken together, all Indian monsoon droughts can thus be linked to slowly-varying oceanic markers: the well-known one in the tropics (El Niño) and the one explored in this work, namely in the midlatitudes (North Atlantic). It is important to note that, in both categories the respective markers appear to be necessary but are not sufficient conditions for the occurrence of a drought. That these drivers are slowly varying offers an avenue for potential improvement in predictability of droughts. While the influence of midlatitudes on the monsoon circulation [34] and ISMR variability [35, 36] has been recognized, the sub-seasonal mechanistic atmospheric bridge unraveled in this study represents a substantial improvement in our understanding of connections between the North Atlantic and Indian monsoon droughts. More pertinently, it points to the need for expanding the existing tropics-centered paradigm of monsoon droughts into a framework that includes extratropical teleconnections [37].

## REFERENCES

- [1] Parthasarathy, B. & Mooley, D. A. Some features of a long homogeneous series of Indian summer monsoon rainfall. *Monthly Weather Review* **106**, 771–781 (1978).
- [2] Yasunari, T. Structure of an Indian summer monsoon system with around 40-day period. *Journal of the Meteorological Society of Japan* **59**, 336–354 (1981).
- [3] Krishnamurthy, V. & Shukla, J. Intraseasonal and interannual variability of rainfall over India. *Journal of Climate* **13**, 4366–4377 (2000).
- [4] Gadgil, S. The Indian monsoon and its variability. *Annual Review of Earth and Planetary Sciences* **31**, 429–467 (2003).
- [5] Hoyos, C. D. & Webster, P. J. The Role of the intraseasonal variability in the nature of Asian monsoon precipitation. *Journal of Climate* **20**, 4402–4424 (2007).
- [6] Sikka, D. Monsoon drought in India. Tech. Rep. 2, COLA/CARE, Maryland, USA (1999).
- [7] Goswami, B. N. South Asian monsoon. In Lau, W. K. M. & Waliser, D. W. (eds.) *Intraseasonal Variability in the Atmosphere-Ocean Climate System*, 21–72 (Springer-Praxis, Chichester, UK, 2005), 2nd edn.
- [8] Gadgil, S. & Gadgil, S. The Indian monsoon, GDP and agriculture. *Economics and Political Weekly* **41**, 4887–4895 (2006).
- [9] Charney, J. G. & Shukla, J. Predictability of monsoons. In Lighthill, J. & Pearce, R. (eds.) *Monsoon Dynamics*, 99–109 (Cambridge University Press, 1981).
- [10] Rajeevan, M., Unnikrishnan, C. K. & Preethi, B. Evaluation of the ENSEMBLES multi-model seasonal forecasts of Indian summer monsoon variability. *Climate Dynamics* **38**, 2257–2274 (2012).
- [11] Nanjundiah, R. S., Francis, P. A., Ved, M. & Gadgil, S. Predicting the extremes of Indian summer monsoon rainfall with coupled ocean-atmosphere models. *Current Science* **104**, 1380–1393 (2013).

- [12] Li, J. & Wang, B. How predictable is the anomaly pattern of the Indian summer rainfall? *Climate Dynamics* **46**, 2847–2861 (2016).
- [13] Rasmusson, E. M. & Carpenter, T. H. The relationship between eastern equatorial Pacific sea surface temperatures and rainfall over India and Sri Lanka. *Monthly Weather Review* **111**, 517–528 (1983).
- [14] Webster, P. J. *et al.* Monsoons: Processes, predictability, and the prospects for prediction. *Journal of Geophysical Research, Oceans* **103**, 14451–1510 (1998).
- [15] Krishna Kumar, K., Rajagopalan, B., Hoerling, M., Bates, G. & Cane, M. A. Unraveling the mystery of Indian monsoon failure during El Niño. *Science* **314**, 115–119 (2006).
- [16] Fan, F. *et al.* Revisiting the relationship between the South Asian summer monsoon drought and El Niño warming pattern. *Atmospheric Science Letters* **18**, 175–182 (2017).
- [17] Varikoden, H., Revadekar, J. V., Choudhary, Y. & Preethi, B. Droughts of Indian summer monsoon associated with El Niño and Non-El Niño years. *International Journal of Climatology* **35**, 1916–1925 (2014).
- [18] Wang, B. & Xu, X. Northern Hemisphere Summer Monsoon Singularities and Climatological Intraseasonal Oscillation. *Journal of Climate* **10**, 1071–1085 (1997).
- [19] Turner, A. G. & Annamalai, H. Climate change and the South Asian summer monsoon. *Nature Climate Change* **2**, 587–595 (2012).
- [20] Li, X. & Ting, M. Recent and future changes in the Asian monsoon-ENSO relationship: Natural or forced? *Geophysical Research Letters* **42**, 3502–3512 (2015).
- [21] Hoskins, B. J. & Yang, G.-Y. The equatorial response to higher-latitude forcing. *Journal of the Atmospheric Sciences* **57**, 1197–1213 (2000).
- [22] Branstator, G. & Teng, J. Tropospheric waveguide connections and their seasonality. *Journal of the Atmospheric Sciences* **74**, 1513–1532 (2017).

- [23] Goswami, B. N., Madhusoodanan, M. S., Neema, C. P. & Sengupta, D. A physical mechanism for North Atlantic SST influence on the Indian summer monsoon. *Geophysical Research Letters* **33**, L02706 (2006).
- [24] Lu, R., Dong, B. & Ding, H. Impact of the Atlantic multidecadal oscillation on the Asian summer monsoon. *Geophysical Research Letters* **33**, L24701 (2006).
- [25] Rajeevan, M. & Sridhar, L. Inter-annual relationship between Atlantic sea surface temperature anomalies and Indian summer monsoon. *Geophysical Research Letters* **35**, L21704 (2008).
- [26] Li, S., Perlwitz, J., Quan, X. & Hoerling, M. P. Modelling the influence of North Atlantic multidecadal warmth on the Indian summer rainfall. *Geophysical Research Letters* **35**, L05804 (2008).
- [27] Wang, C., Kucharski, F., Barimalala, R. & Bracco, A. Teleconnections of the tropical Atlantic to the tropical Indian and Pacific Oceans: A review of recent findings. *Meteorologische Zeitschrift* **18**, 445–454 (2009).
- [28] Krishnamurthy, L. & Krishnamurthy, V. Teleconnections of Indian monsoon rainfall with AMO and Atlantic tripole. *Climate Dynamics* **46**, 2269–2285 (2016).
- [29] Sabeerali, C. T., Ajayamohan, R. S., Bangalath, H. K. & Chen, N. Atlantic zonal mode: An emerging source of Indian summer monsoon variability in a warming world. *Geophysical Research Letters* **46**, 4460–4467 (2019).
- [30] Minobe, S., Luwano-Yoshida, A., Komori, N., Xie, S.-P. & Small, R. J. Influence of the Gulf Stream on the troposphere. *Nature* **452**, 206–211 (2008).
- [31] Smirnov, D. *et al.* Investigating the local atmospheric response to a realistic shift in the Oyashio sea surface temperature front. *Journal of Climate* **28**, 1126–1147 (2015).
- [32] Willis, S. M., Thompson, D. W. J. & Ciasto, L. M. On the observed relationships between variability in Gulf Stream sea surface temperatures and the atmospheric circulation over the North Atlantic. *Journal of Climate* **29**, 3719 (2016).

- [33] The June and August episodes in NEN + Dr years (blue curve in Fig. S9b) are strong enough to make the seasonal response (Fig. 3) seem like a deep tropospheric cyclonic circulation. .
- [34] Bordoni, S. & Schneider, T. Monsoons as eddy-mediated regime transitions of the tropical overturning circulation. *Nature Geoscience* **1**, 515–519 (2008).
- [35] Krishnan, R., Kumar, V., Sugi, M. & Yoshimura, J. Internal feedbacks from monsoon-midlatitude interactions during droughts in the Indian summer monsoon. *Journal of the Atmospheric Sciences* **66**, 553–578 (2009).
- [36] Yadav, R. K. Role of equatorial central Pacific and northwest of North Atlantic 2-metre surface temperatures in modulating Indian summer monsoon variability. *Climate Dynamics* **32**, 549–563 (2009).
- [37] Stan, C. *et al.* Review of tropical-extratropical teleconnections on intraseasonal time scales. *Reviews of Geophysics* **55**, 902–937 (2017).
- [38] Rayner, N. A. *et al.* Global analyses of sea surface temperature, sea ice, and night marine air temperature since the late Nineteenth century. *Journal of Geophysical Research* **108**, 4407 (2003).
- [39] Parthasarathy, B., Munot, A. A. & Kothawale, D. R. Monthly and seasonal rainfall time series for all India, homogeneous divisions and meteorological subdivisions, 1871-1994. Tech. Rep. RR065, Indian Institute of Tropical Meteorology, Pune, India (1996).
- [40] Poli, P. *et al.* ERA-20C: An Atmospheric Reanalysis of the Twentieth Century. *Journal of Climate* **29**, 4083–4097 (2016).
- [41] Ross, S. *Probability and Statistics for Scientists and Engineers* (Elsevier Academic Press Europe, 2009), 4th edn.

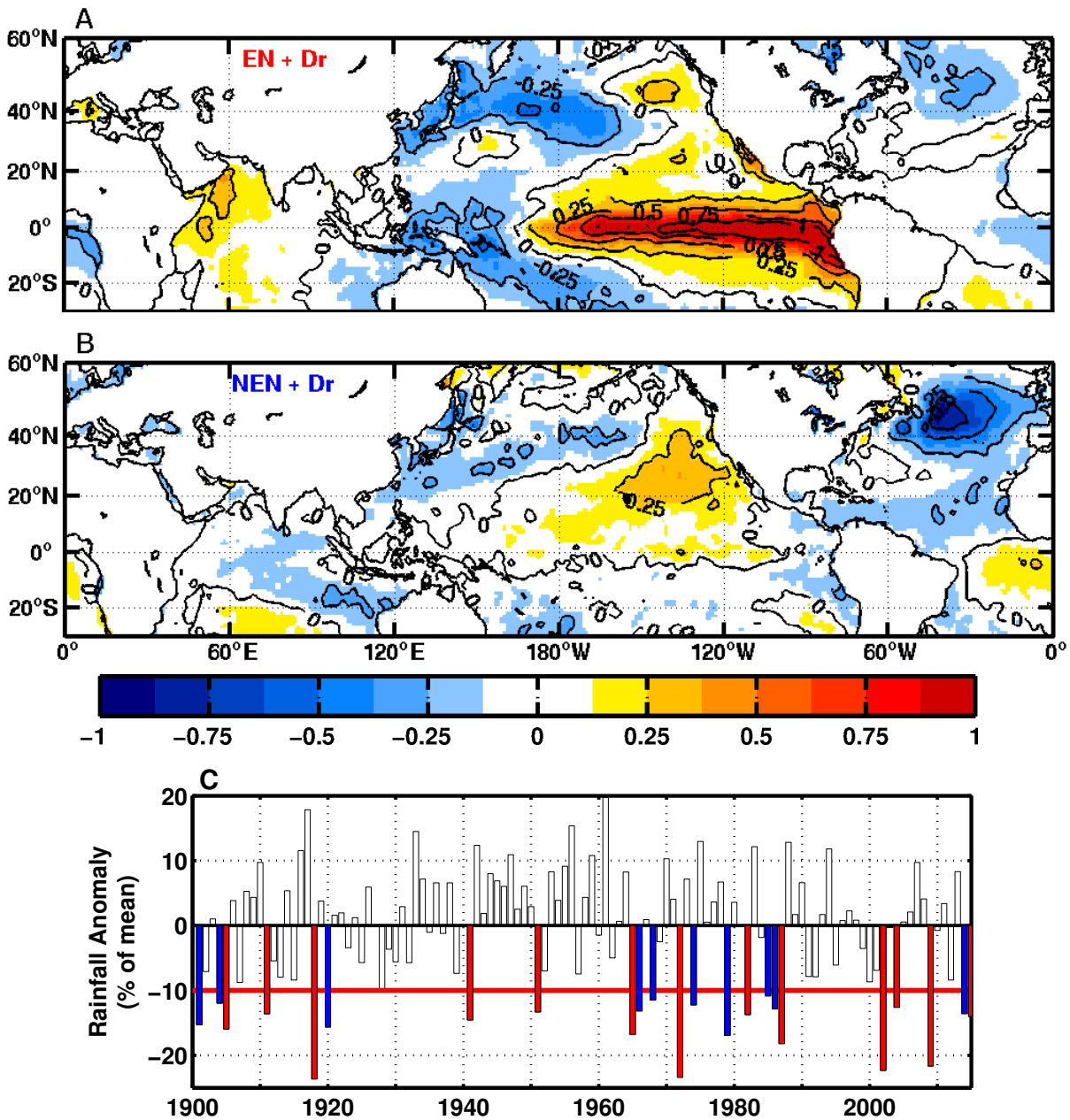


**Fig. 1:** Spatial distribution of anomalies of detrended JJAS sea surface temperature (SST) for the two types of Indian monsoon droughts: (A) EN + Dr; (B) NEN + Dr. The detrending is based on removal of a linear trend for 1901-2015 at each grid-location, and the maps shown are the average of fluctuations around the trend, for the years listed in [Table S1](#). Based on the  $1^\circ$ , monthly SST product from the Hadley Centre [39]. Colorbar is in  $^\circ\text{C}$ . (C) Interannual variation of anomalies of seasonal (JJAS) monsoon rainfall based on the IITM homogeneous Indian monthly rainfall dataset [38] for the period 1901-2015. The horizontal red line at -10% denotes the threshold for defining a drought, as per the India Meteorological Department (IMD). The departures marked in red (blue) indicate droughts that occurred during an El Niño (no El Niño) year.

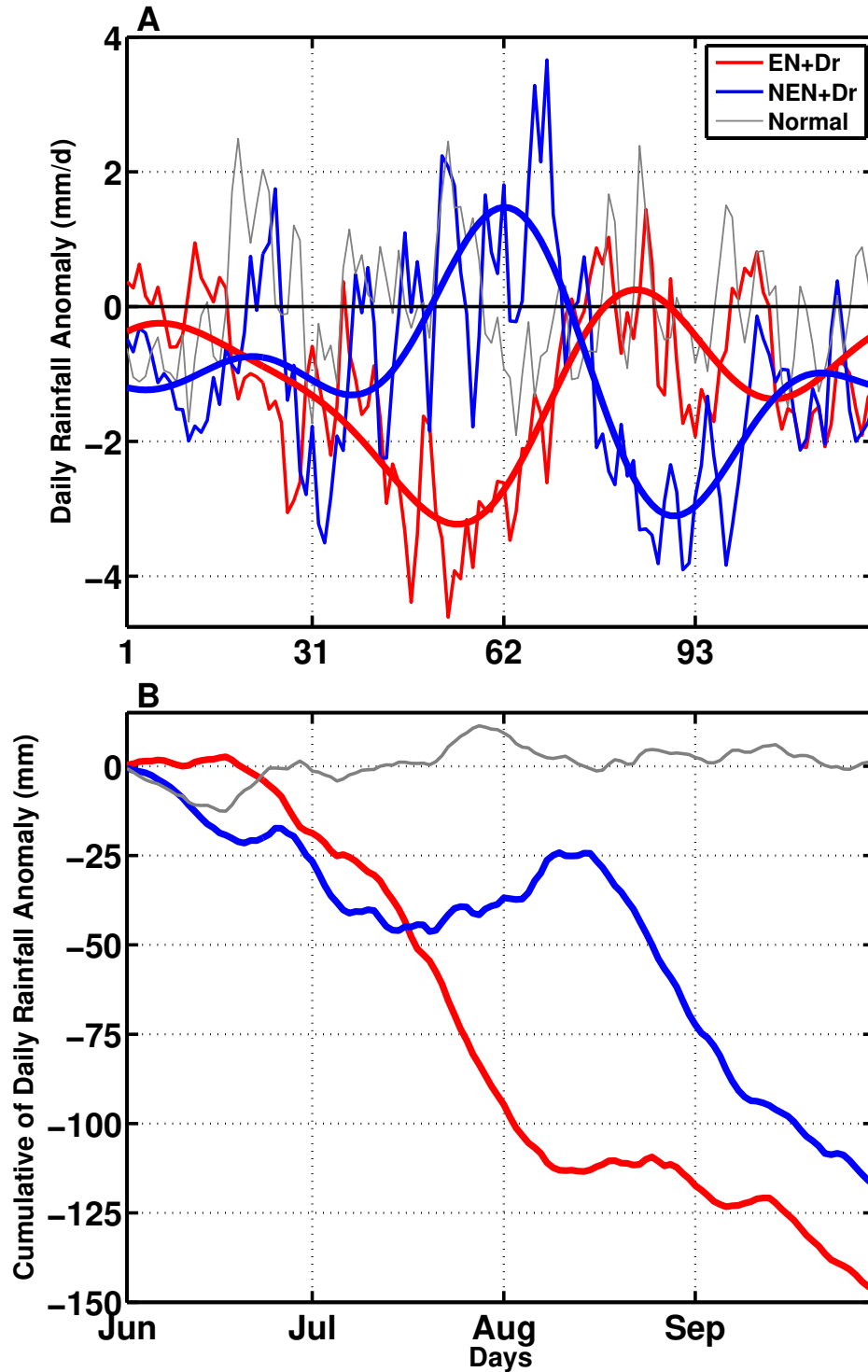


**Fig. 2:** (A) Temporal evolution of anomalies of daily area-averaged rainfall over central India (16.5N-26.5N, 74.5E-86.5E; land-only) during JJAS, for the two categories of droughts, along with their respective leading three harmonics ( $\sim 120, 60, 40$  days; thick red and blue). The thin red and blue curves shown are an average of daily anomalies of 13 EN + Dr and 10 NEN + Dr years listed in [Table S1](#). (B) Cumulative of daily rainfall anomalies shown in (A). The average of daily rainfall anomalies for a normal year (based on 18 randomly chosen years with seasonal rainfall anomaly between -5% and 5%) and its cumulative are shown as a grey line in both panels. Based on IMD gridded 1-degree, daily rainfall data from 1901-2015.

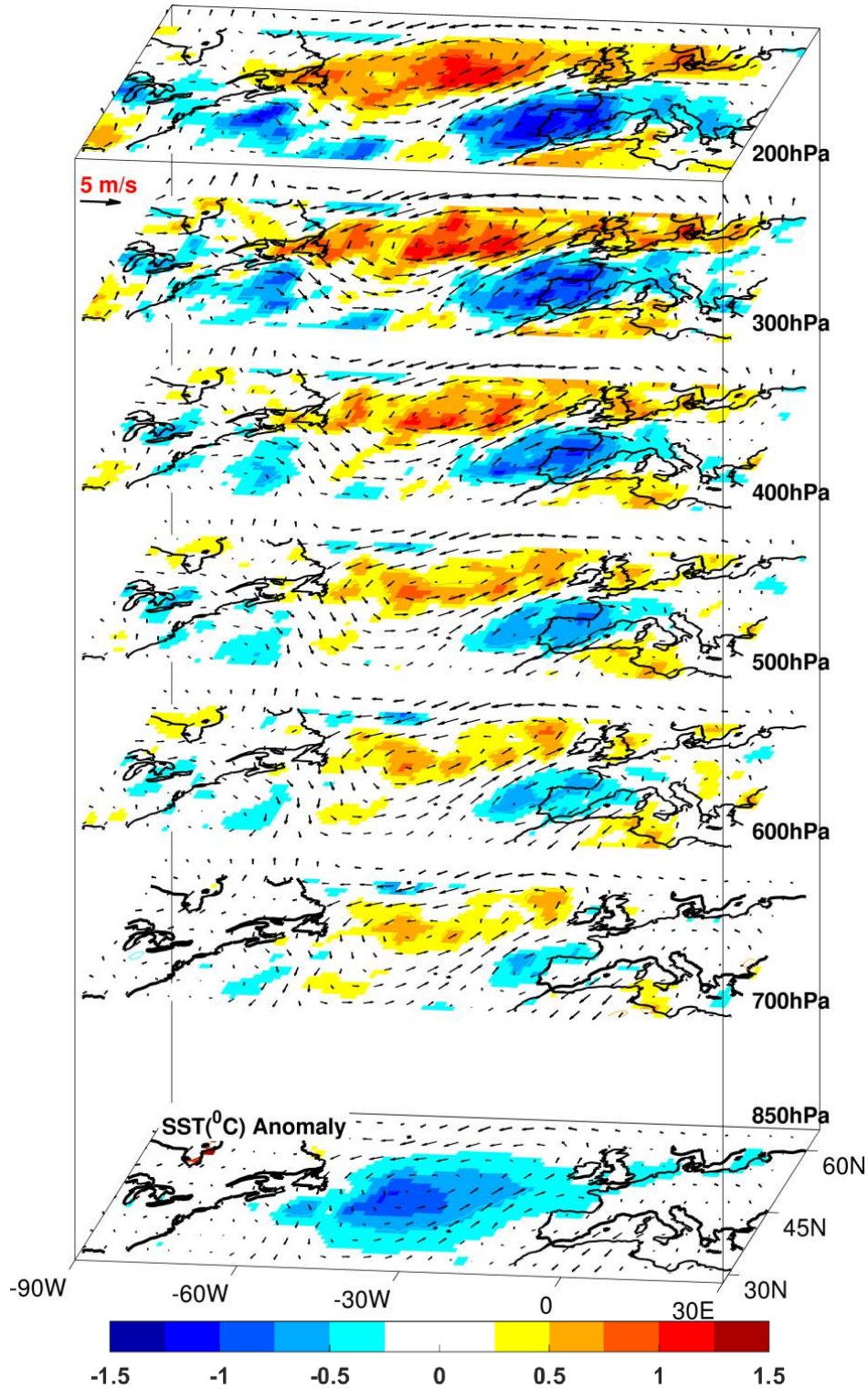


**Fig. 3:** Composites of anomalies of JJAS mean wind (vectors) and vorticity (shading) in the free troposphere, based on NEN + Dr years; the shading in the bottom-most panel represents SST anomaly. The colorbar applies to both vorticity ( $\times 2 \times 10^5$ ) and SST. The wind and vorticity anomalies are based on ERA 20th Century Reanalysis data [41], and SST anomalies are based on the  $1^\circ$ , monthly SST product from the Hadley Centre [39]. See Methods section for the construction of composites.

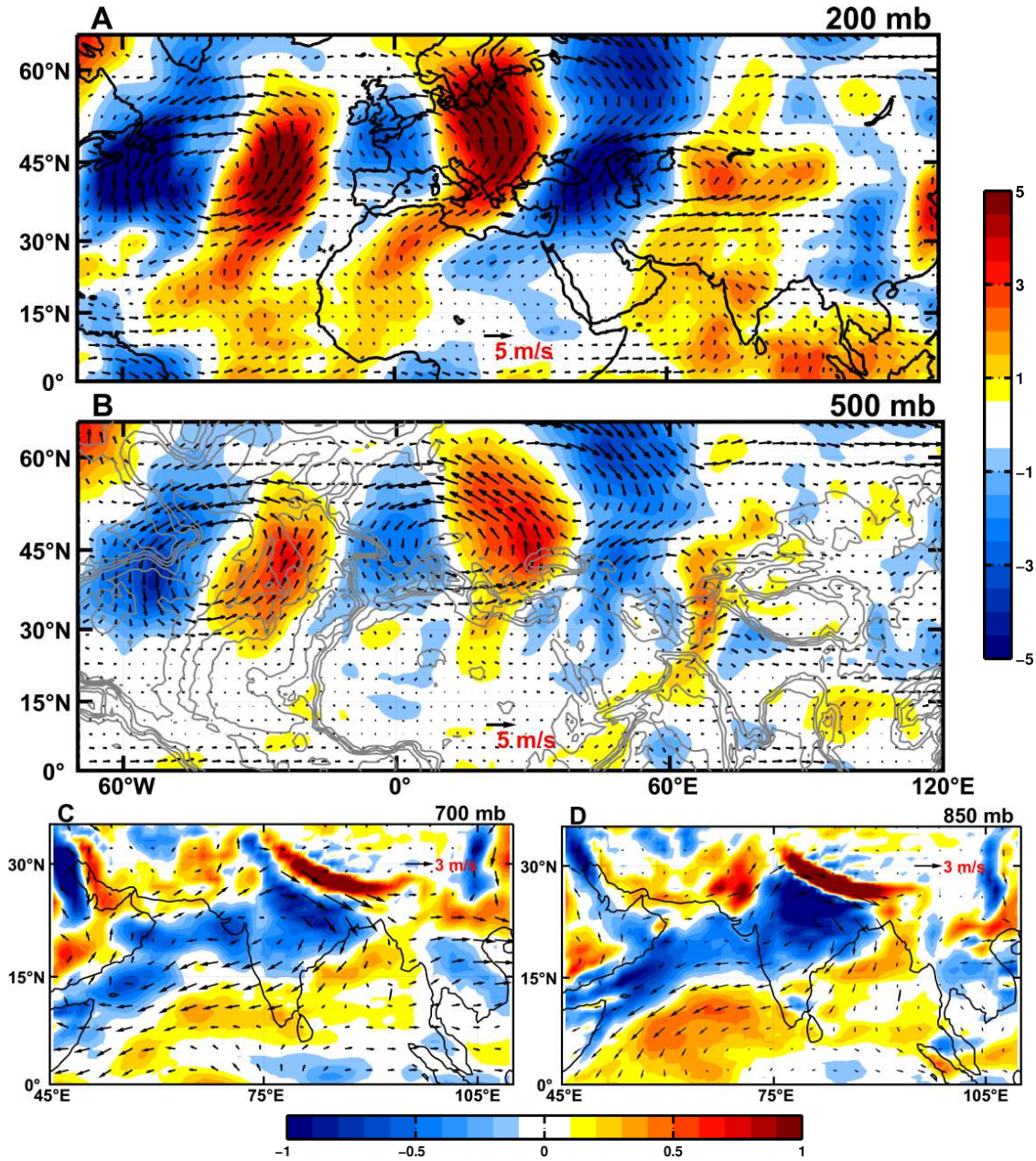


**Fig. 4:** Composites of anomalies of (top two panels) wind (vectors) and meridional velocity (shading) at (A) 200 mb and (B) 500 mb during the first half of the break (days 81-90; see blue curve in Fig. 2b) in the Indian monsoon rainfall; and (bottom two panels) wind (vectors) and vorticity ( $\times 10^5$ ; shading) at (C) 700 mb and (D) 850 mb, based on the respective break periods late in the season for each of the NEN+Dr years. The gray lines in the 500 mb panel represent topography. Based on ERA 20th Century Reanalysis data [41]. See Methods section for the construction of composites.

# Supplementary Material

## Data and Methods

### Data

- *Rainfall*: 1901-2015, daily, 1° gridded rainfall dataset from the India Meteorological Department (IMD). This product can be obtained from [www.imd.gov.in](http://www.imd.gov.in).
- *Sea Surface Temperature (SST)*: 1901-2015, monthly, 1° gridded Had-SST from the Hadley Centre, UK Met Office [39]. This dataset can be obtained from <https://www.metoffice.gov.uk/hadobs/hadsst3/data/download.html>.
- *ERA 20C*: 1901-2010, daily, 1° gridded zonal and meridional winds and vorticity. This product [41] can be obtained from <https://www.ecmwf.int/en/forecasts/datasets/reanalysis-datasets/era-20c>.

### Methods

- *Identifying El Niño Years*: El Niño years were identified by an inspection of anomalies of detrended SST during JJAS. Post-1950 events were confirmed based on estimates from the Climate Prediction Center, NOAA, and can be accessed via “El Niño / La Niña → Historical Information” at <https://www.cpc.ncep.noaa.gov/>.
- *Detrended SST Anomalies*: A linear trend in JJAS mean SST is removed at each location for the period 1901-2015, and fluctuations around the trend composited for the years of interest.
- *Rainfall, Wind and Vorticity Anomalies*: If  $F(x, y, d, yr)$  represents rain, wind or vorticity at a location  $(x, y)$  on day  $d$  during JJAS, in year  $yr$ , then the daily anomalies at each location are estimated as:  $F_{\text{anom}}(x, y, d, yr) = F(x, y, d, yr) - F_{\text{clim}}(x, y, d)$  where  $F_{\text{clim}}(x, y, d) = \frac{1}{N} \left[ \sum_{yr=1}^{yr=N} F(x, y, d, yr) \right]$ . The anomalies of *area-averaged rainfall* (e.g., Fig. 2a) are estimated by calculating daily area-averaged rainfall and then subtracting the corresponding daily climatology. *Seasonal anomalies* of  $F$  (e.g., Fig. 3 or Fig. 4) can be estimated either by subtracting JJAS means from the corresponding seasonal climatology, or by averaging the daily anomalies  $F_{\text{anom}}(x, y, d, yr)$  over JJAS.

- *Composites:* The ERA20C data is available up to 2010 and hence 2014 was not included in the wind and vorticity composites. Furthermore, the composites presented have been constructed based on the anomalies of 7 of the 9 NEN + Dr years for which the reanalysis data is available. This is because the lower level (850 mb) circulation features over the Indian region are not consistent with the observed IMD rainfall during the break periods for two of the early era years (1901 and 1904). This could be either because of the quality of early era IMD observations or the fidelity of reanalysis data (the years being close to spin-up period [41]).

## Supplementary Text

**Intra-category Heterogeneity.** The rainfall evolution for each of the droughts suggests considerable intra-category heterogeneity. The spread in normal years (grey dashed lines in Figs. S3b and S3d) is substantially lower than in either of the drought categories. Moreover, Fig. S3d indicates that NEN + Dr can be near-normal until as late as end of July/early August, before the abrupt transition to an eventual drought.

**Anomalously Cold North Atlantic and No Indian Monsoon Drought.** It is interesting to note that the evolution of the cumulative curves for the two categories, namely {NEN + Droughts} (blue in Fig. S7b) and {North Atlantic SST < 0 but no drought} (cyan in Fig. S7b) are nearly the same until mid-August. The circulation features resulting in an early season (June) break in the latter category are shown in Fig. S8. The June break mechanism is very similar to that seen in mid-to-late August for NEN + Dr (Fig. 4). In other words, a cool North Atlantic sets up a vorticity forcing and its interaction with the upper-level flow (Fig. S8a) results in a wave train that eventually leads to an anticyclonic circulation over the Indian land mass (Fig. S8c). Thus, it appears that *two breaks* are needed during a cold episode of the North Atlantic for the Indian monsoon to go into a drought-like state (see also Fig. S9).

The **statistical significance** of JJAS daily total columnar vorticity anomalies during NEN + Dr years is established via a suite of three tests (Table S3). The first test shows that these anomalies are significantly different from the long-term mean (zero by definition) in a seasonal sense with a  $p$ -value  $\approx 10^{-7}$ . The second and third tests are more stringent and involve a comparison with years when the North Atlantic is “cold” (SST anomaly <  $-0.25^{\circ}\text{C}$ ; Fig. S9a) and there is a preference for a cyclonic environment (Fig. S9b). Here too, the columnar vorticity anomalies are significantly different both in a seasonal as well as an episodic sense, with  $p$ -values of 4.6% and 0.3%, respectively.

## SUPPLEMENTARY FIGURES

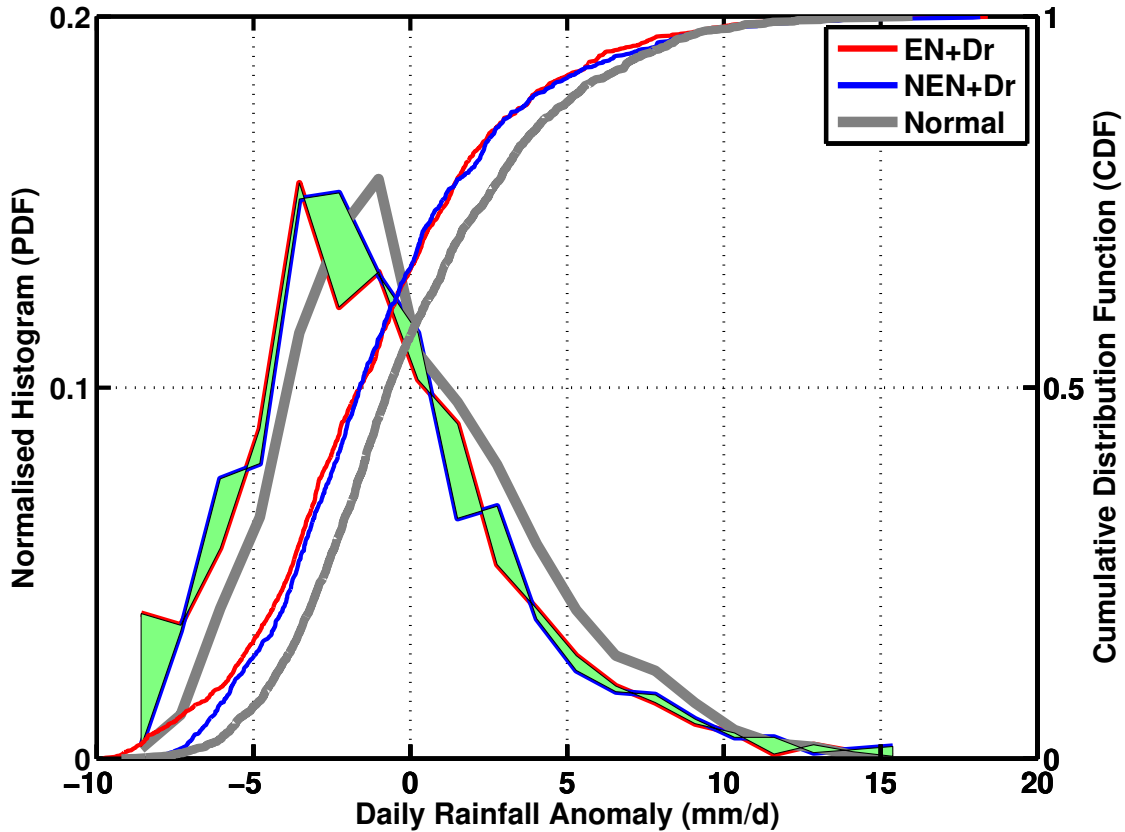


**Fig. S1:** Normalized histograms (shown as line curves) and cumulative distribution functions (CDF) of anomalies of daily area-averaged rainfall over central India (16.5N-26.5N, 74.5E-86.5E; land only; also, see also Methods section) for EN + Dr (red), NEN + Dr (blue) and normal (gray). The light-green shading highlights the difference between the two kinds of droughts as well as their difference between them and a normal year. The CDFs of EN + Dr (red) and NEN + Dr (blue) are statistically indistinguishable at 5% significance level ( $p$ -value of 0.09), but are both significantly different from a normal year (gray “S” curve;  $p$ -value  $< 10^{-5}$ ). The empirical CDFs have been compared using a two-sample Kolmogorov-Smirnov test with a null hypothesis that they are indistinguishable [40].

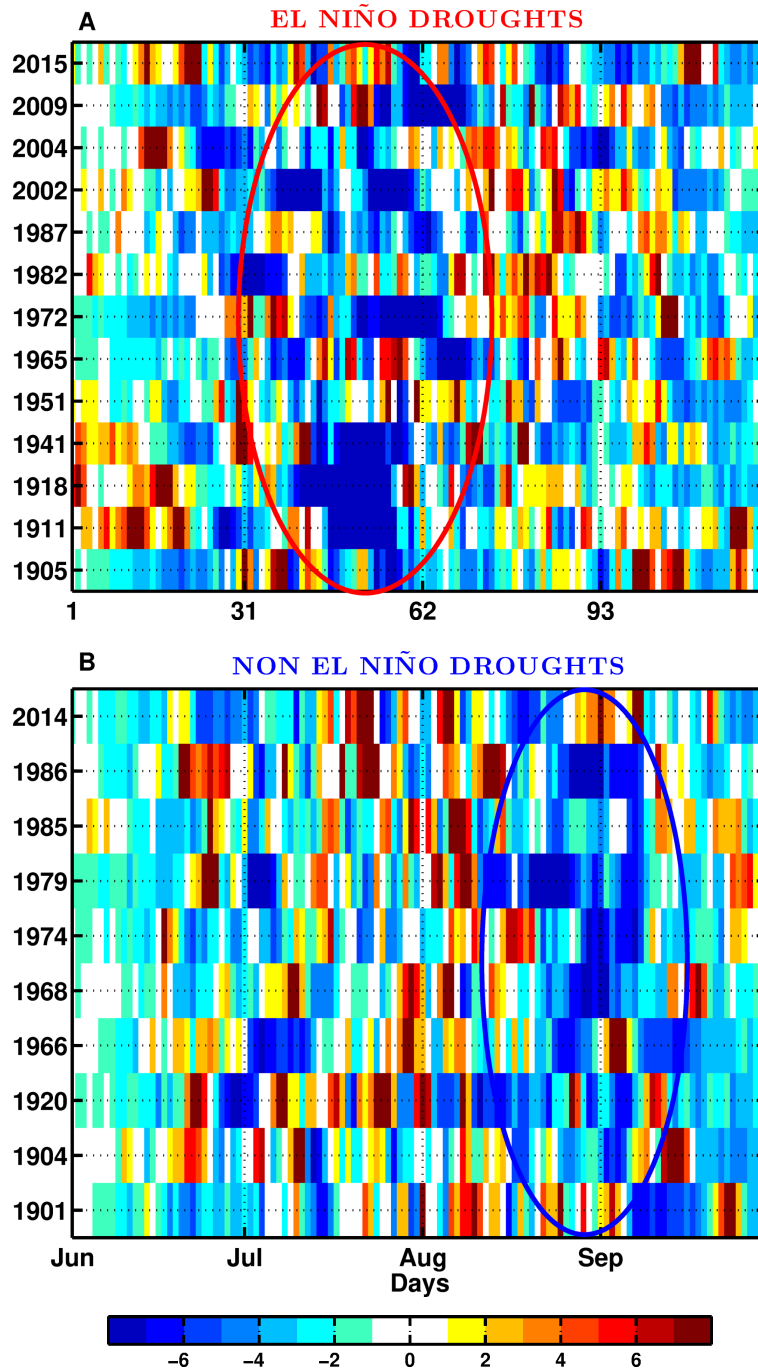


**Fig. S2:** Time series of anomalies of daily area-averaged rainfall (mm/d) over central India (16.5N-26.5N, 74.5E-86.5E; land only; see also Methods section), during JJAS, shown with a color-coding, for each of the drought years during (A) an El Niño year (EN + Dr) and (B) a non El Niño year (NEN + Dr). The red and blue ellipses are used to highlight the tendency of long breaks to cluster in different times of the season, in the two kinds of droughts. Colorbar is in mm/d. The average of these time series is shown as thin red and blue curves, respectively, in Fig. 2a.

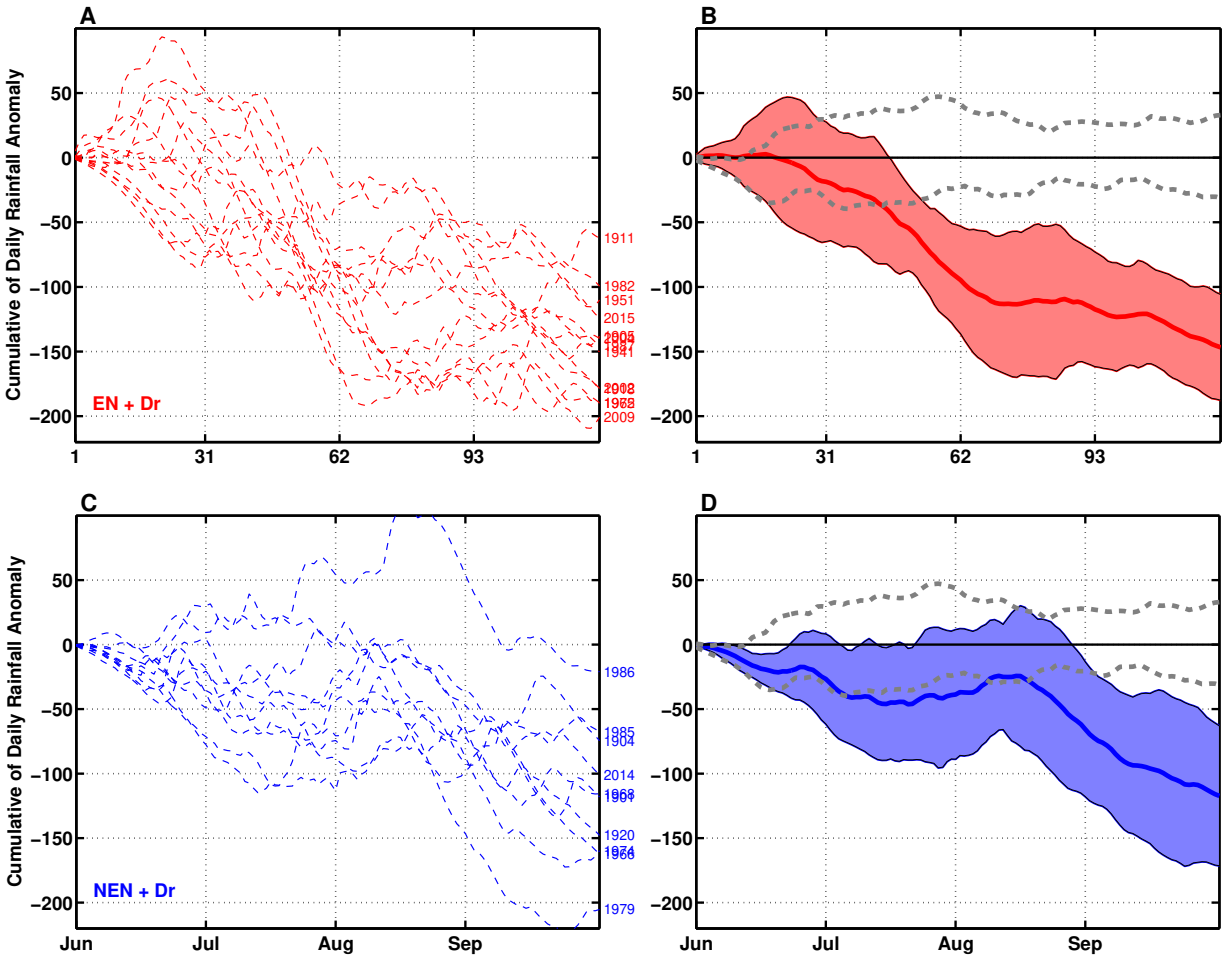


**Fig. S3:** Cumulative curves of daily anomalies of area-averaged rainfall over central India (16.5N-26.5N, 74.5E-86.5E; land only; see also Methods section) for each of the drought years belonging to the two categories, along with the respective average cumulative curves: (A, B) EN + Dr and (C, D) NEN + Dr. The corresponding spread ( $\pm 1$  standard deviation) in each of the categories is shown as a shading in panels (B) and (D). The standard deviation is estimated based on 13 EN + Dr and 10 NEN + Dr years. The dashed gray lines in panels (B) and (D) correspond to the spread ( $\pm 1$  standard deviation) of 18 normal years. The solid red and blue curves in (B, D) are the same as the ones shown in Fig. 2b.

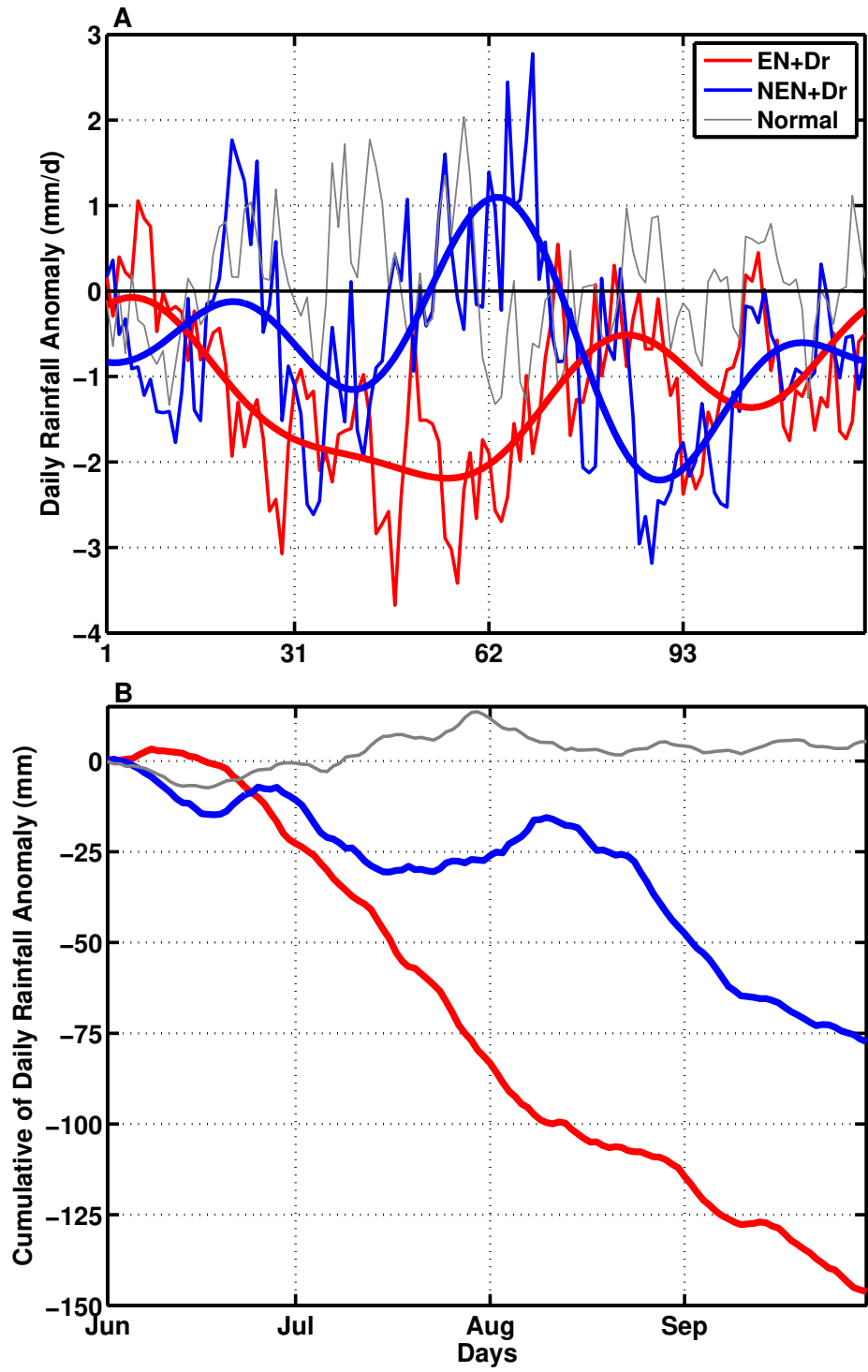
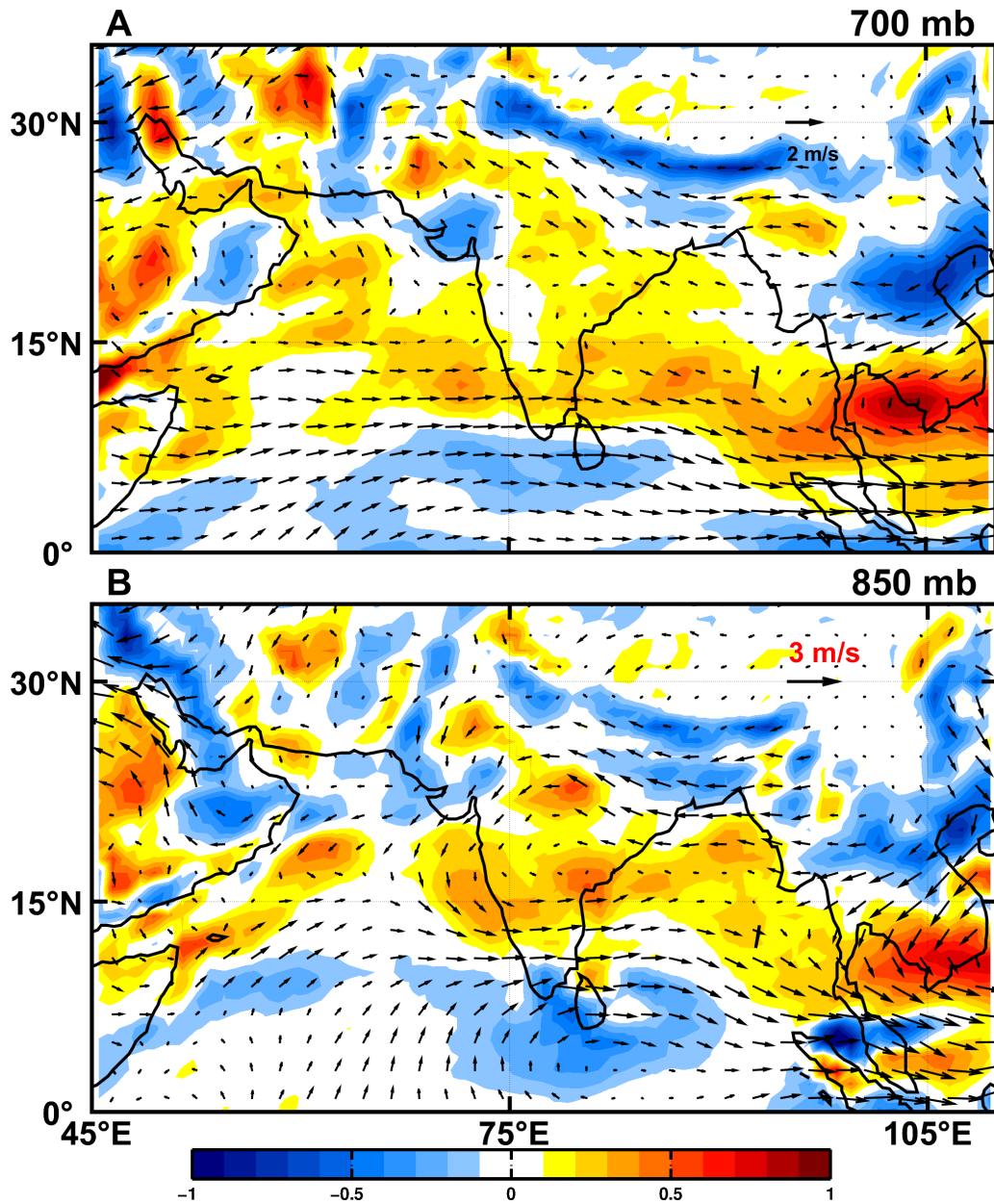
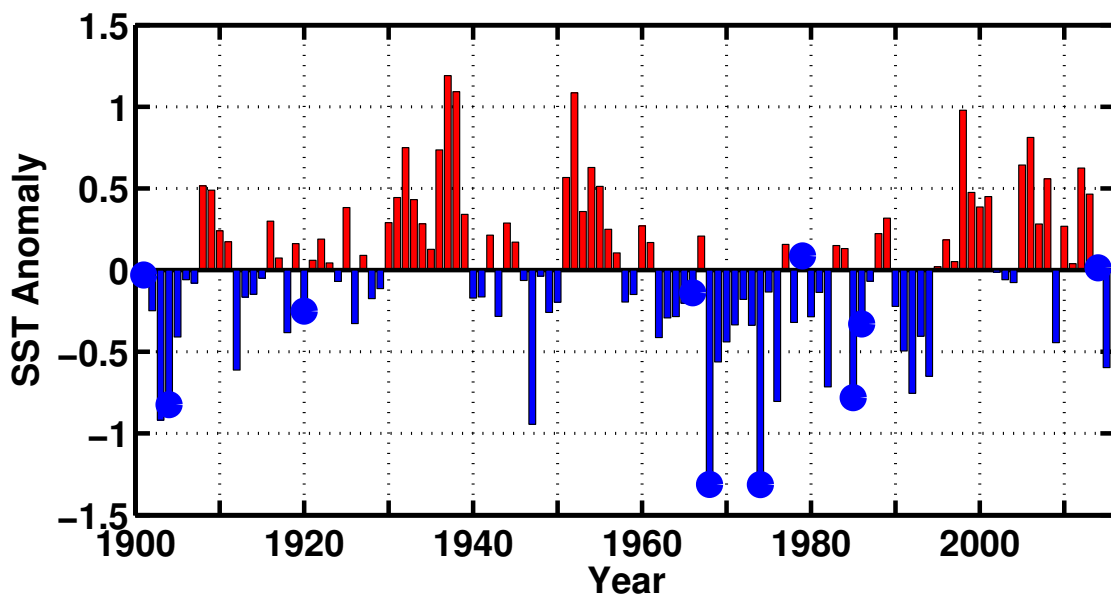


Fig. S4: Same as in Fig. 2, but for area-averaged all-India rainfall.



**Fig. S5:** Composites of anomalies of wind (vectors) and vorticity ( $\times 10^5$ ; shading) at (A) 700 mb and (B) 850 mb, during the 20-day period prior to the long break (see blue ellipse in Fig. S2B) in NEN+Dr years. Legend for arrows is shown in panel (B). Based on ERA 20th Century Reanalysis data [41]. See Methods section for the construction of composites.



**Fig. S6:** Long-term (1900-2015) time series of the North Atlantic (35N-55N; 310E-340E; based on Fig. 1b) SST anomalies ( $^{\circ}\text{C}$ ) with the 10 NEN drought years marked as blue filled circles. Based on the  $1^{\circ}$ , monthly SST product from the Hadley Centre [39].

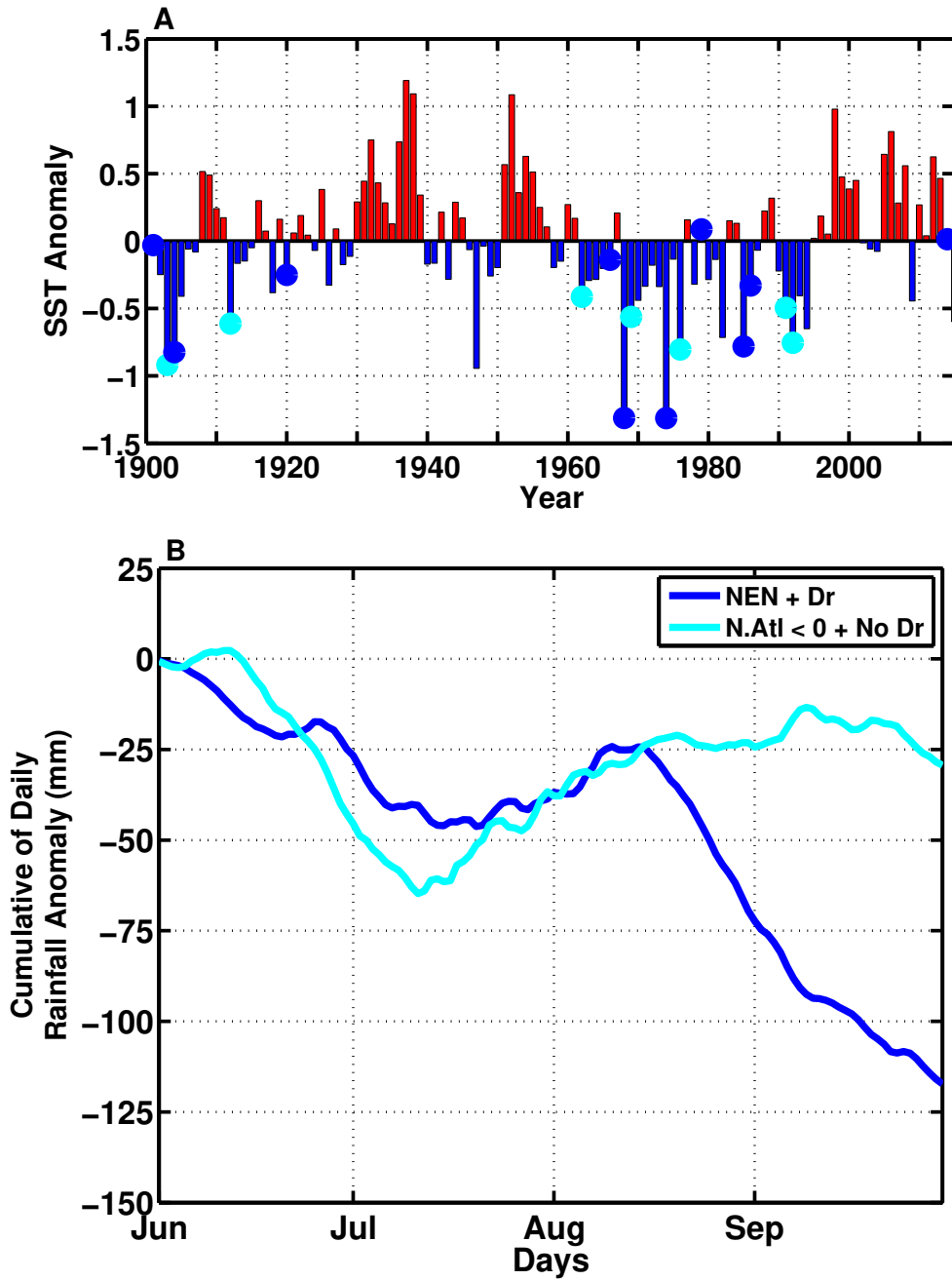


**Fig. S7:** (A) Same as in Fig. S6 but also showing 7 no-drought years when the North Atlantic was negative as cyan filled circles (see Table S2). (B) Cumulative of anomalies of daily area-averaged rainfall over central India (as in Fig. 2b) for NEN + Dr years (blue circles in (A)) and North Atlantic SST < 0 + no drought years (cyan circles in (A)).

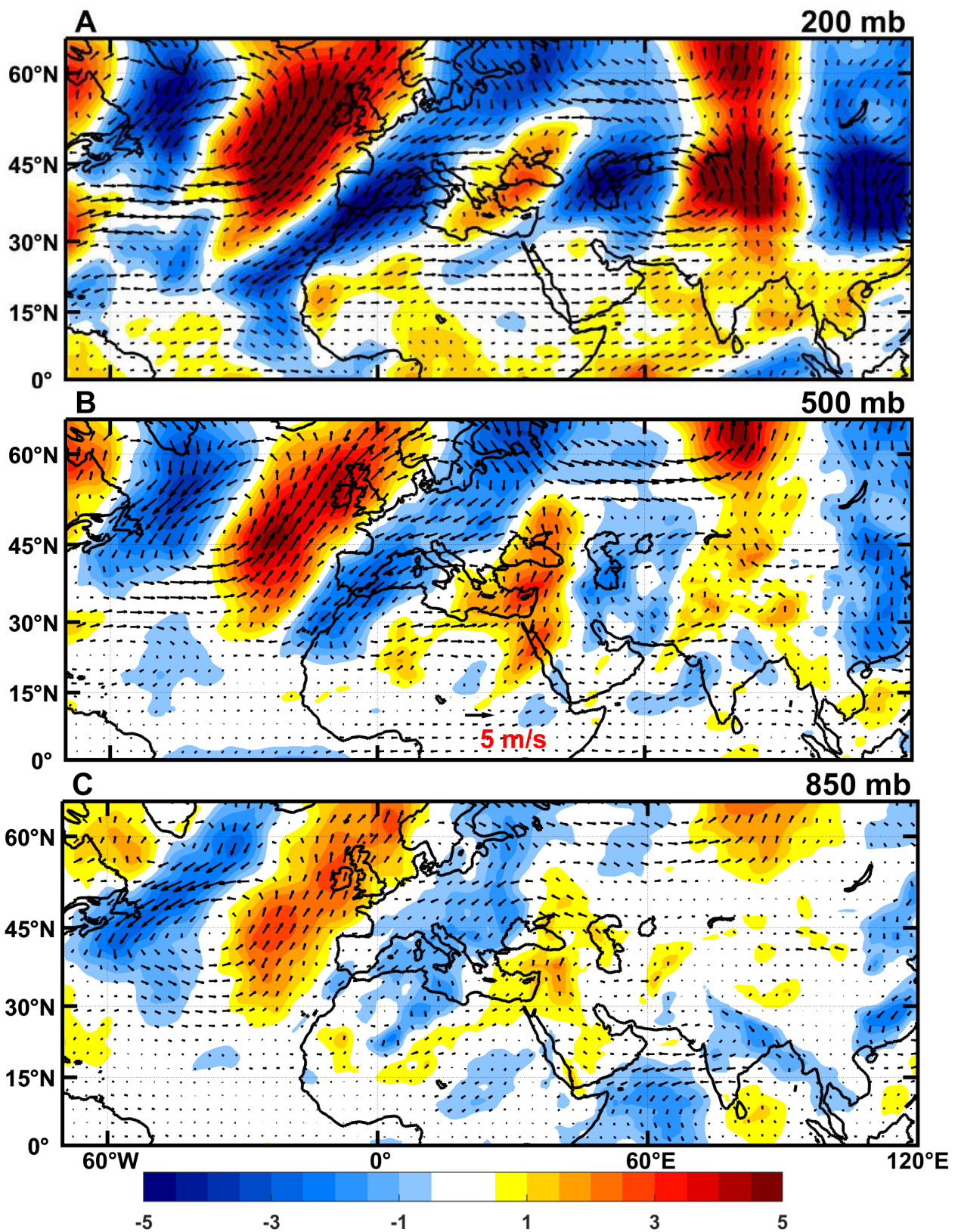


**Fig. S8:** Composite of anomalies of wind (vectors) and meridional velocity (shading) at (A) 200 mb; (B) 500 mb; and (C) 850 mb, during days 20-30 (i.e., Jun 20-30) for the years listed in [Table S2](#) and shown as cyan filled circles in [Fig. S7a](#). These days are based on the early-season dip in the cyan curve shown in [Fig. S7b](#). Legend for arrows is shown in panel (B).

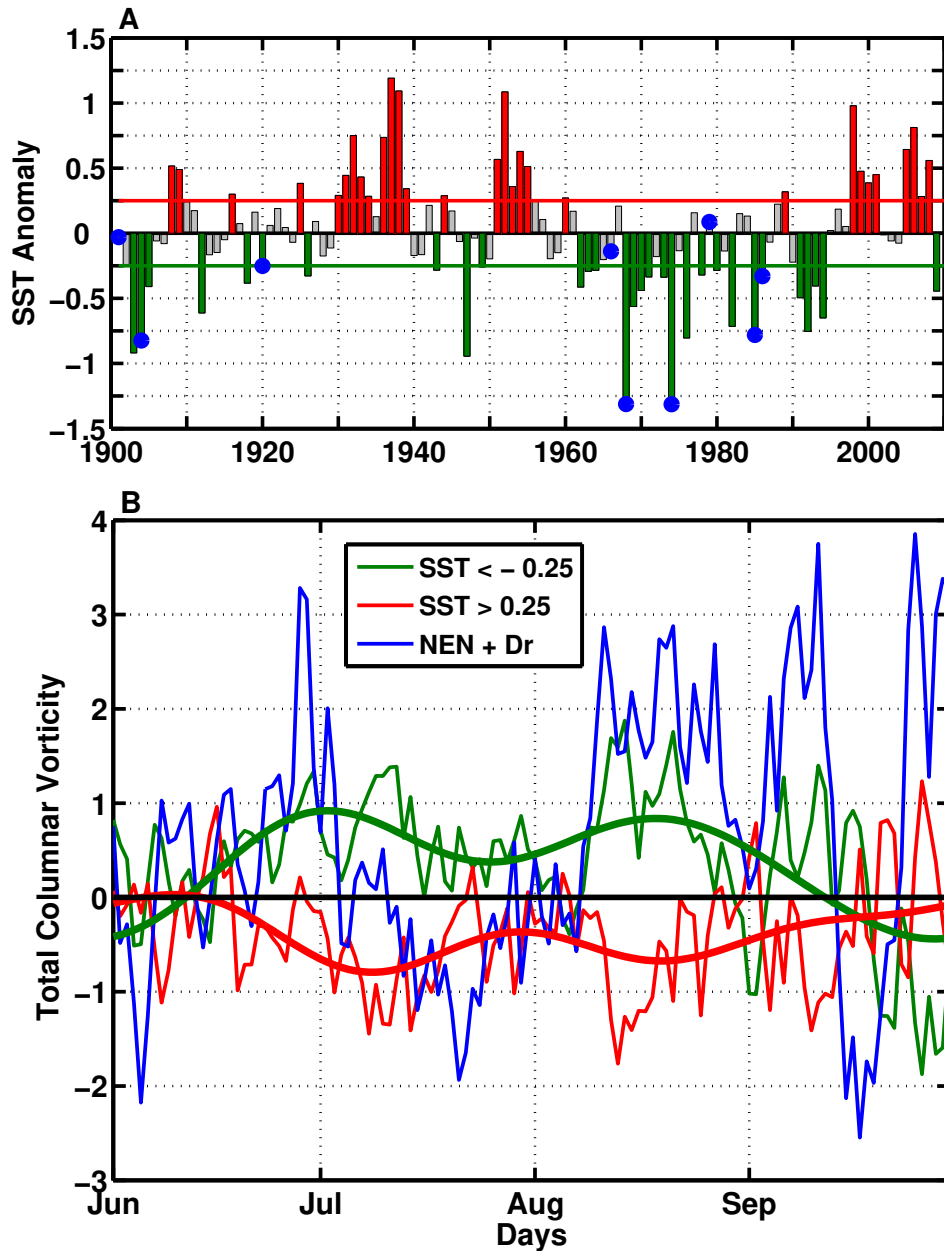


**Fig. S9:** (A) Long-term (1900-2009) time series of the North Atlantic SST anomalies (averaged over 35N-55N; 310E-340E with NEN droughts marked as blue filled circles). The red and green bars represent “warm” and “cold” years when the SST anomaly is  $> 0.25^{\circ}\text{C}$  and  $< -0.25^{\circ}\text{C}$  ( $\approx$  half the standard deviation of long-term SST data), respectively. Each of these categories comprise of approximately 30 years. (B) Time series of anomalies of daily total columnar (200, 300, 500 and 700 mb) vorticity ( $\times 10^5$ ) averaged over this area during JJAS, composited over the “warm” and “cold” years. The thick red and green curves represent the respective first three harmonics. Time series of anomalies of daily total-columnar vorticity over the North Atlantic box for NEN + Dr years is shown in blue.

## SUPPLEMENTARY TABLES

**Table S1:** The list of Indian monsoon years where the seasonal (June through September; JJAS) rainfall anomaly is less than -10% of the long-term (1901-2015) mean, and is classified as a drought. The anomalies shown are based on the IITM homogeneous Indian monthly rainfall dataset [38] for the period 1901-2015. The droughts that occurred during an El Niño (no El Niño) year are marked in red (blue) (see also Fig. 1c).

Year	Seasonal Rainfall Anomaly (% of long-term mean)
1901	-15
1904	-12
1905	-16
1911	-14
1918	-24
1920	-16
1941	-15
1951	-13
1965	-17
1966	-13
1968	-11
1972	-23
1974	-12
1979	-17
1982	-14
1985	-11
1986	-13
1987	-18
2002	-22
2004	-13
2009	-22
2014	-14
2015	-14

**Table S2:** Years when the North Atlantic SST (averaged over 35-55N, 310-340E) during JJAS was negative, but did not result in an Indian monsoon drought, and the corresponding seasonal rainfall anomaly.

Year	North Atlantic SST Anomaly (°C)	Indian Monsoon Seasonal Rainfall Anomaly (% of long-term mean)
1903	-0.9	1
1912	-0.6	-5.4
1962	-0.4	-5
1969	-0.6	-2.5
1976	-0.8	0.5
1991	-0.5	-7.9
1992	-0.7	-7.9

**Table S3:** Statistical significance of anomalies of daily total columnar vorticity during 9 NEN + Dr years (Fig. S9b; see also “Supplementary Text”).  $\mu$  represents “population” mean,  $\bar{V}_N$  and  $S_{V_N}$  represent the sample mean and standard deviation of  $N$  years of daily observations for the period of interest (in bold in column 1) during JJAS. “Cold” years represent those years when the North Atlantic SST anomaly  $< -0.25^\circ\text{C}$  (see Fig. S9a). All tests are based on a  $t$ -distribution. The second and third tests are based on a two-sample  $t$ -test for comparing means [40].

Description	Hypothesis	Sample Statistics	Test Statistic Value	$p$ -value
<b>Test1:</b> Comparison with long-term <b>JJAS</b> mean (2-sided)	$H_0: \mu_\omega = 0$ $H_1: \mu_\omega \neq 0$	$\bar{V}_9 = 6.3 \times 10^{-6}$ $S_{V_9} = 4 \times 10^{-5}$ $N = 9 \times 122 = 1098$	5.2	$2P( t_{1097}  > 5.2)$ $\approx 0$
<b>Test2:</b> Comparison with <b>JJAS</b> mean during “cold” North Atlantic years (1-sided)	$H_0: \mu_\omega^{\text{NEN+Dr}} = \mu_\omega^{\text{Cold}}$ $H_1: \mu_\omega^{\text{NEN+Dr}} < \mu_\omega^{\text{Cold}}$	$\bar{V}_9 = 6.3 \times 10^{-6}$ $\bar{V}_{30} = 3.7 \times 10^{-6}$ $S_{V_9} = 4 \times 10^{-5}$ $S_{V_{30}} = 4.5 \times 10^{-5}$ $N_9 = 9 \times 122 = 1098$ $N_{30} = 30 \times 122 = 3660$	1.7	$P(t_{N_9+N_{30}-2} > 1.7)$ $\approx 4.6\%$
<b>Test3:</b> Comparison with <b>August episode mean (days 70-90)</b> during “cold” North Atlantic years (1-sided)	$H_0: \mu_\omega^{\text{NEN+Dr}} = \mu_\omega^{\text{Cold}}$ $H_1: \mu_\omega^{\text{NEN+Dr}} < \mu_\omega^{\text{Cold}}$	$\bar{V}_9 = 1.9 \times 10^{-5}$ $\bar{V}_{30} = 0.97 \times 10^{-5}$ $S_{V_9} = 3.4 \times 10^{-5}$ $S_{V_{30}} = 4 \times 10^{-5}$ $N_9 = 9 \times 21 = 189$ $N_{30} = 30 \times 21 = 630$	2.8	$P(t_{N_9+N_{30}-2} > 2.8)$ $\approx 0.3\%$

## REFERENCES

- [38] B. Parthasarathy, A. A. Munot, D. R. Kothawale, Monthly and seasonal rainfall time series for all India, homogeneous divisions and meteorological subdivisions, 1871-1994, *Tech. Rep. RR065*, Indian Institute of Tropical Meteorology, Pune, India (1996).
- [39] N. A. Rayner, *et al.*, *J. of Geophys. Res.* **108**, 4407 (2003).
- [40] S. Ross, *Probability and Statistics for Scientists and Engineers* (Elsevier Academic Press Europe, 2009), 4th edition.
- [41] P. Poli, *et al.*, *J. of Clim.* **29**, 4083 (2016).